Applications in Energy and Combustion Science 6 (2021) 100029

Contents lists available at ScienceDirect

Applications in Energy and Combustion Science

journal homepage: www.elsevier.com/locate/jaecs

Influence of plasma-assisted ignition on flame propagation and performance in a spark-ignition engine

Joonsik Hwang[a,b,1], Wooyeong Kim[a], Choongsik Bae[a,*]

[a] Department of Mechanical Engineering, Korea Advanced Institute of Science and Technology (KAIST), Republic of Korea
[b] Center for Advanced Vehicular Systems (CAVS) & Department of Mechanical Engineering, Mississippi State University, Mississippi 39762, United States

ARTICLE INFO

Keywords:
Non-thermal plasma
Microwave
Lean-burn
Spark ignition engine
Flame kernel

ABSTRACT

Lean-burn is an attractive concept for reasons of high thermal efficiency and low nitrogen oxide (NO_x) emissions, however, successful implementation in spark-ignition (SI) engines turned out to be challenging because of misfire or partial burn caused by attenuated flame propagation. In order to overcome this issue, microwave-assisted plasma ignition system (MAPIS) has been applied in combustion systems. The MAPIS consists of a conventional ignition coil, a non-resistor spark plug, a mixing unit, a waveguide, and a magnetron (2.45GHz, 3kW). A series of experiments was carried out to understand discharge characteristics and to validate its performance in a constant volume vessel as well as in a single-cylinder spark-ignition engine. The fundamental investigation based on optical emission spectroscopy and flame imaging showed that the ejection of the microwave was beneficial to produce more reactive species such as OH and O radicals thanks to higher electron temperature than conventional spark ignition. The lean limit was able to be extended up to an equivalence ratio of 0.5 based on a larger initial flame kernel size with MAPIS in the vessel test. Meanwhile, in the engine test, combustion stability was noticeably improved showing smaller cycle-to-cycle fluctuations in in-cylinder pressure. Improvement in fuel efficiency up to 6% could be achieved by stable operation under fuel-lean conditions. In terms of emissions, MAPIS was advantageous to reduce carbon monoxide (CO) emissions by promoting more complete combustion.

Abbreviations

Abbreviations

aTDC	After top dead center
bTDC	Before top dead center
CAD	Crank angle degree
CCD	Charge coupled device
CO	Carbon monoxide
COV	Coefficient of variation
DC	Direct current
EGR	Exhaust gas recirculation
RF	Radio frequency
GDI	Gasoline direct injection
IGBT	Insulated gate bipolar transistor
IMEP	Indicated mean effective pressure
MAPIS	Microwave-assisted plasma ignition system
NO_x	Nitrogen oxide
TCI	transistorized coil ignition

1. Introduction

In the spark-ignition (SI) engines, combustion is initiated by the high-temperature thermal plasma kernel between spark plug electrodes. Sufficiently high electrical potential induces breakdown followed by the arc and glow discharge. After spark started, electrons are accelerated by the electric field and highly active radicals/ionized gas molecules are created. Then, the consecutive exothermic chemical reactions in the flame front allow self-sustaining flame propagation. There are different types of standard ignition systems including coil ignition system, capacitive-discharge ignition (CDI) system, and magneto ignition system. Among them, the most prevailing ignition system in SI engines is the transistorized coil ignition (TCI) system because of its cost-effectiveness and robustness. In modern gasoline direct injection (GDI) engine, advanced a technologies such as turbocharger, high-tumble/swirl motion, exhaust gas recirculation (EGR), and lean-burn strategies have been adopted to achieve high efficiency with low pollutant emissions [1, 2, 3, 4]. However, the application of these concepts causes unfavorable ambient conditions for flame propagation. For example, in the lean-burn regime, flame propagation is attenuated by flame quenching due to insufficient

* Corresponding author.
E-mail address: csbae@kaist.ac.kr (C. Bae).
[1] Now at Center for Advanced Vehicular Systems (CAVS) & Department of Mechanical Engineering, Mississippi State University, USA.

https://doi.org/10.1016/j.jaecs.2021.100029
Received 4 November 2020; Received in revised form 25 March 2021; Accepted 25 April 2021
Available online 7 May 2021

Nomenclature

α	Thermal diffusivity [m2/s]
E	Electric field [V/m]
h_c	Heat of combustion [J/kg]
$\dot{m}'''_F$	Product generation rate [kg/s•m3]
N	Gas density [m−3]
P	In-cylinder pressure [MPa]
Q	Heat from the system [J]
R_{crit}	Critical flame radius [m]
γ	Ratio of specific heat [a.u.]
S_L	Laminar flame speed [m/s]
t	Time [s]
V	In-cylinder volume [m3]

heat generation in the flame, so it often results in a misfire or partial burn. There have been advancements in standard ignition systems to resolve this issue by increasing stored electrical energy or applying multi-discharge [5, 6, 7].

In the meanwhile, another approach so-called volumetric ignition using a non-thermal plasma mechanism has gained attention as an alternative ignition method for future GDI engines. Different from the thermal plasma, the heat losses and thermal loading on the ignition system are no longer issues in the non-thermal plasma because only the electrons are highly excited than ions and neutrals. In this way, chemical reactions can be enhanced by more efficient energy transfer between electron and reactive species. Even though the system cost is not comparable to the TCI system, it has been demonstrating a great potential for combustion improvement [8, 9]. Thus many researchers have been developing non-thermal ignition systems such as streamer discharge, surface ignition, nanosecond pulsed dielectric barrier discharge, and high-frequency resonance plasma ignition to combustion systems, however, the realization of non-thermal plasma in real engine turned out to be challenging because of the often failures to generate stable non-thermal plasma under high ambient pressure condition [10, 11, 12]. Therefore, a hybrid concept using both of the conventional TCI system and non-thermal plasma has been developed by Ikeda at el [13]. It uses a microwave-assisted plasma ignition system (MAPIS) that consists of conventional TCI system and microwave source. The ignition is initiated by TCI and then expanded by microwave ejection in the discharge region. The application of MAPIS system has been successful in the engine system by showing extended lean limit, lower fuel consumption, and lower emission characteristics compared to TCI system [12, 14, 15, 16]. The electron temperature and reduced electric field (*E/N*, electric field/molecular number density) in plasma are known to have substantial effects on combustion [17]. The non-thermal plasma is known to have higher electron temperature and is more kinetically active because of the rapid production of active radicals and excited species by electron impact dissociation, excitation, and subsequent energy relaxation [18]. In terms of this aspect, since the MAPIS system is using TCI system for the ignition and expansion by microwave, the enhancement in electron temperature and reduced electric field is smaller than non-thermal plasma such as radio frequency or nanosecond pulse systems, however, it has the better discharge stability that ensured by TCI system under entire engine conditions [19].

In this study, we aim to establish a comprehensive understanding of microwave effects and electrode geometry on flame enhancement. Especially since the MAPIS system can be further combined with other ignition concept, for instance flame jet ignitor and high-energy TCI system, the influence of electrode geometry on flame enhancement by microwave should be understood. The discharge characteristics for both TCI and MAPIS system were analyzed by optical emission spectroscopy (OES) to acquire temperature data in the discharge region. The investigation was carried out with a MAPIS system based on an ignition system introduced by Ikeda at al [20, 21]. Each single component in the MAPIS was carefully designed based on efficiency and energy balance analysis. The MAPIS was tested in a constant volume combustion vessel and a single cylinder GDI engine. Initial flame was visualized by high-speed shadowgraph and OH radical imaging. A series of comparison between two ignition systems; TCI and MAPIS was performed based on flame development, combustion phase, fuel efficiency, and emission characteristics under various engine speed, engine load, equivalence ratio, and microwave application energy. The remaining content of the manuscript is organized as follows: the experimental methods are described, detailing the MAPIS component, the constant volume vessel, high-speed optical imaging, and single-cylinder SI engine. The results section presents energy flow, discharge characteristics, followed by the flame imaging and engine performance and emission characteristics.

2. Test setup and condition

2.1. MAPIS components

The MAPIS can be categorized into four main sections: power source, transmission system, power monitoring system, and igniter. A schematic diagram of the entire system is presented in Fig. 1. Detailed specification and working mechanism are described in following section.

2.1.1. Power sources: magnetron and ignition coil

A continuous-wave (CW) magnetron (National, NL 10250-1) was utilized to generate a microwave with a frequency of 2.45 GHz. The internal structure of the magnetron is illustrated in Fig. 2 [22]. The inset of the figure indicates the trajectory of a free electron in the magnetron. Cathode located at the center of a vacuum tube is surrounded by a specific cavity shape that determines the frequency of microwave. The cathode is at low potential (-5kV in this study) compared to the anode. Due to this potential difference, free electrons are emitted from the cathode by thermionic emission. The free electrons are then accelerated toward the anode by the electric field. In this situation, the free electrons do not travel straight from cathode to anode, however, they travel in a spiral direction because of a magnetic field applied by an external magnet. In other words, circumferential force (Lorentz force) was applied by the combination of electric and magnetic fields in the vacuum tube. The spiral movement of free electrons induces swirling electron clouds [23]. When the electron clouds pass the resonating cavities, they create a high-frequency electromagnetic field, and finally, this energy is transmitted by an output coupling loop (antenna). The microwave source utilized in this study was CW magnetron, however, a custom-made triggering circuit controlled 5kV DC with an insulated gate bipolar transistor (IGBT) was used to operate the magnetron in pulsed mode. To characterize the electric behavior of the magnetron, voltage, and current was monitored as shown in Fig. 3. It is emphasized that this measurement is for electric energy used to generate microwave, not the microwave energy delivered to the igniter. The microwave energy was measured by a power meter at each component and the measurement of microwave power will be described in the following section. Time after operating command started is presented in the x-axis. A 5V TTL command with 20μs pulse duration was delivered to the magnetron driving circuit and 5kV of voltage was applied to the magnetron. Considering a few picoseconds response scale of IGBT, the increase of the voltage and current indicated a certain delay for microwave generation. A peak of a current (discharge) can be seen in 5μs after the command signal was applied. It implies that there was the time required to heat the filament and achieve thermionic emission from the cathode. The sudden peak of the current also indicates there was discharge between the cathode and anode in the vacuum tube. After 8μs, the voltage and current were stabilized for the period of approximately 20μs. The time delay of 8μs shown by voltage and current measurement was consistent with the power meter that showed power generation after 8μs later than the start of the command signal. This is attributed to the rotating electron clouds in the resonant

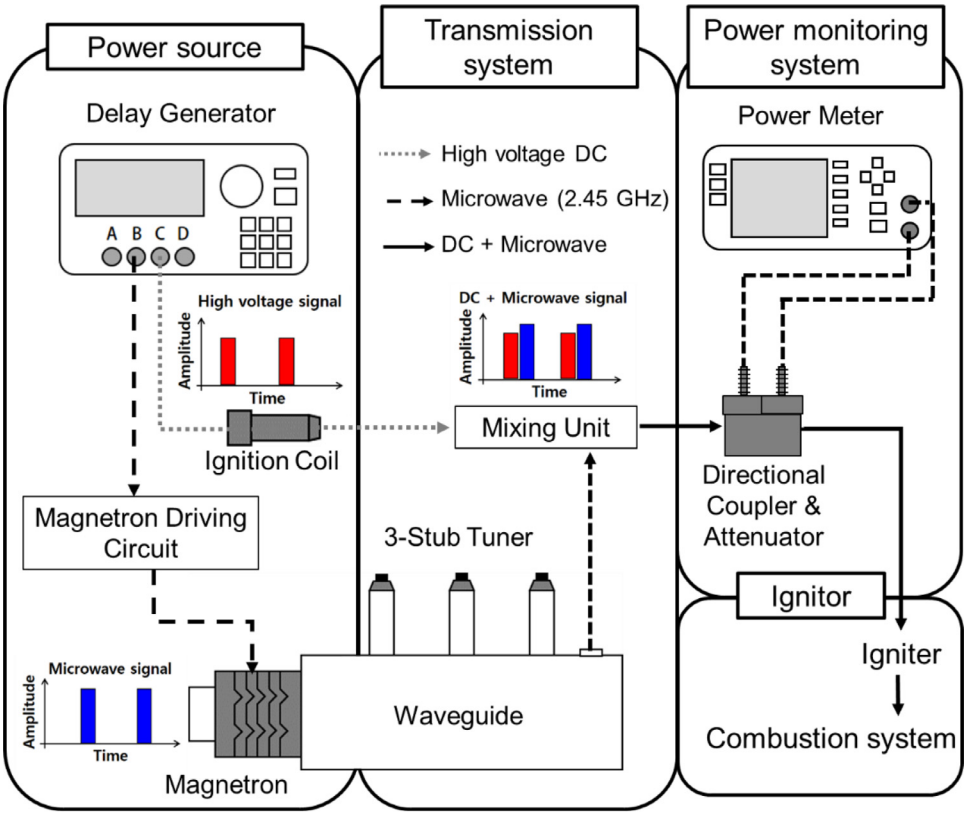

Fig. 1. Schematic diagram of MAPIS.

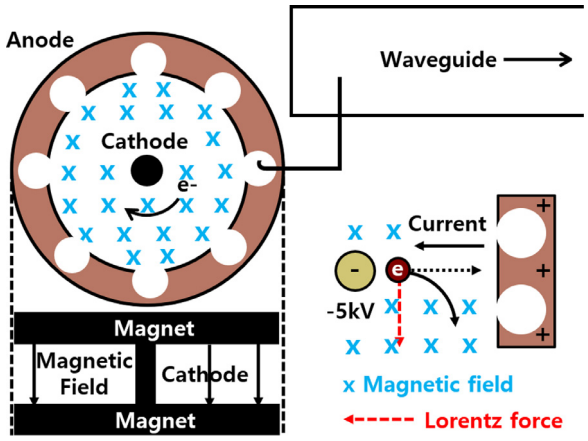

Fig. 2. Internal structure of magnetron (reproduced from [22]).

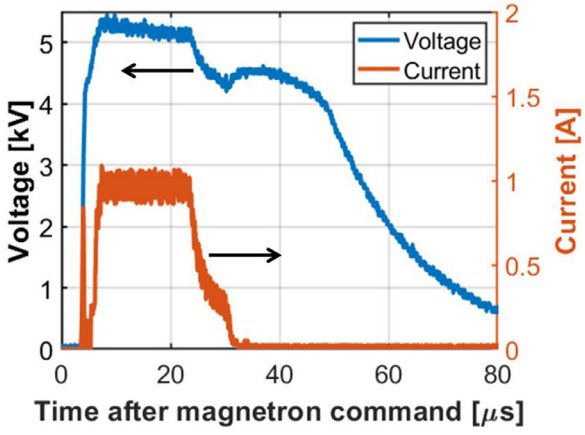

Fig. 3. Measured voltage and current of magnetron.

cavities. An interesting feature in this voltage and current profile, they dropped slowly, for example, the current was continued longer than the input command signal of 20μs. The possible reason for this is that the rotating electron clouds in the cavity had a certain momentum that kept current even after the operating signal terminated.

The igniter was not designed to initiate the flame propagation only by the microwave however, the actual discharge was controlled by a conventional spark ignition coil (Denso, 27300-3F100). It basically uses electrical energy stored in the inductance of a coil. There are two coils existed: primary winding has relatively few turns of heavy wire, meanwhile, the secondary winding consists of thousands of turns of thinner wire. Before the ignition event, the system switches current on the primary winding that builds magnetic field in the coil. When the current stops at the primary winding, it produces high voltage across the secondary windings as the magnetic field is disappeared. This high voltage DC was delivered to the igniter for the start of flame propagation. To evaluate spark energy, voltage and current were measured at the spark plug. Fig. 4 shows the voltage and current profiles with a 1ms of coil charging time. It is noted that the spark energy (in this case 60mJ) can be acquired by integrating this voltage and current curve according to time. The electrical potential between the central and ground electrode was initially increased until breakdown that is followed by arc phase and glow discharge. The duration of energy dissipation by discharge process was kept to 1ms by input coil charging time. It is known that the breakdown phase has the lowest heat loss approximately 5% of electric energy to heat losses, however, total energy taken by this period is less than 1% of total discharge energy [24]. Most of the discharge energy is dissipated by the arc and glow discharge that has 70% of heat losses to electrodes since the flame is already far beyond the spark re-

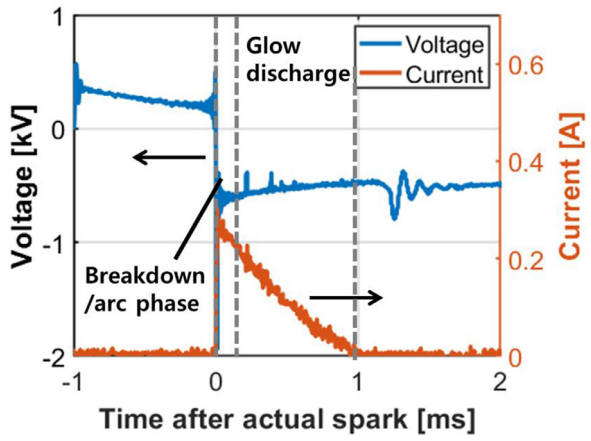

Fig. 4. Measured voltage and current of spark plug.

gion [24]. Therefore, an increase of discharge energy with a longer coil charging time is not helpful to create a larger initial kernel.

2.1.2. Transmission system: waveguide, 3-stub tuner, and mixing unit

To transfer microwave energy generated by the magnetron, a hollow rectangular tube (commercial waveguide) was installed directly to the magnetron. The waveguide was manufactured to have a transverse electric mode (TE_{010}) that has the strongest electric field long the centerline. In the middle of the waveguide, a 3-stub tuner (ASTeX, AX3041) was installed to ensure the maximum transfer efficiency by matching impedance between the microwave source and the following components. In the aspect of the microwave, the shape of the propagating space determines the circuit impedance, so the maximum transmitting power was ensured by deforming the space in the waveguide using 3 rods in the tuner. The procedure to match the impedance was to find maximum power (monitored by a power meter) by trying various combinations of 3 rods settings. The microwave after the tuner was transmitted to the mixing unit through an antenna installed 30mm away from the end of the waveguide.

Two different sources of the microwave and the high voltage DC by the conventional ignition coil and the magnetron were properly mixed by a custom-build mixing unit. The concept of the mixing unit is to prevent leakage of each source but transmit mixed energy only to igniter. For example, in Fig. 1, if the high voltage DC is transferred to the magnetron system, it will create discharge somewhere in the system and fail to ignite mixture in the combustion chamber. Similarly, if the microwave energy is transferred to the ignition coil, it will cause electric failure. Thus, the mixing unit was developed with a pair of parallel plate capacitor and a coil (RF choke) to block the high voltage DC and the microwave, respectively. The components were mounted on a printed circuit board that has 2mm thickness.

2.1.3. Power monitoring system: directional coupler and attenuator

The discharge energy by ignition coil can be measured by voltage and current profiles, however, this method is not applicable for microwave energy measurement. This is because not only it is an electromagnetic wave (not a simple DC) but also a contact of any measuring device completely alters the impedance of the circuit. Therefore, a power meter (Agilent, E4417A) was utilized to measure microwave energy delivered to each component. This power measurement was achieved through a directional coupler. Directional coupler enabled monitoring of transmitted and reflected power. In principle, a perfect impedance matching between the component was challenging especially in the engine application where the space is limited, a portion of applied microwave energy always reflected. By using the directional coupler, the final transmitted microwave power was calculated by subtracting reflected power from the input power. To protect the power meter from accidentally applied high power of the microwave, two attenuators (−55 dB) were installed between the directional coupler and the power meter.

2.1.4. Igniter

A resistor in conventional spark plugs does not allow microwave transmission so non-resistor spark plugs were designed using an in-house numerical simulation code. In each design step, the scattering parameter (S-parameter) defined by eq-1, was carefully evaluated since it determines energy transmission efficiency. For example, if the ratio of the transmitted power to input power is 1 (transmission efficiency of 100%), S-parameter is 0.

$$S-parameter = 10 \cdot \log\left(\frac{P_{transmitted}}{P_{input}}\right) \quad (1)$$

where P_{input} is input microwave power to a component, $P_{transmitted}$ is microwave power after the component. The S-parameter depends on the frequency of the electromagnetic wave, material, channel size, and shape. As there were inevitable constraints in the spark plug design such as igniter size limited by spark plug thread on the engine cylinder head, S-parameter near 0 could not be achieved. In theory, the best scenario was to utilize Teflon material for an insulator with 0.1mm diameter central electrode, however, alumina with 1mm diameter electrode (Inconel pin) was utilized to prevent gas leakage through a gap between the central electrode and the insulator.

A combined high voltage DC and microwave energy were delivered to the igniter. The high voltage DC was transmitted through the central electrode, meanwhile, the microwave was transmitted through a space between the central electrode and shield around the insulator. A conceptual mechanism for the ignition enhancement process is presented in Fig. 5. Before the spark was applied for the actual start of flame kernel formation, the microwave was ejected. Then, ignition is initiated by using a conventional ignition coil. In this situation, expansion of thermal plasma could be enabled by the interaction between free electrons and alternating electromagnetic wave (with the frequency of 2.45 GHz) so it can create a larger initial ignition kernel [26]. After the spark is applied, flame propagation occurs in the field that has an oscillating microwave.

In this study, five different igniters were designed to investigate the influence of ground electrode shape on flame enhancement. Fig. 6 illustrates the schematics of igniters tested in the combustion vessel. The designs were intended to have larger microwave energy deposition by enclosing the discharge area with electrodes. In other words, the primary goal was to minimize microwave leakage from the discharge region. As starting from the conventional spark configuration, the discharge region got enclosed more by installing more electrodes. In the experiment, the input spark energy and microwave energy were set as identical for all the spark configurations.

2.2. Experimental setup

2.2.1. Constant volume vessel

Two main experimental campaigns were carried out in the constant volume combustion vessel: OES and high-speed flame imaging. A spectrometer (Ocean Optics, Maya2000) was used to analyze light intensity according to wavelength in the discharge. The grating (HC-1) installed in the spectrometer has blaze wavelengths at 300 and 600 nm with 300 grooves/mm density and it provides a measurement range of 200-1100 nm wavelength with 1.38 nm resolution. The spectrometer was factory-calibrated with calibration light sources; a deuterium halogen lamp (Ocean Optics, DH-3P-CAL) for 200-1100 nm and a tungsten halogen lamp (Ocean Optics, HP-3plus-CAL) for 400-1100 nm additionally. Natural lights from surroundings were blocked to measure the light spectrum only from the discharge. The data was acquired with an exposure time of 200ms and 10 times of repetition. The light intensity for nitrogen radical showed the maximum variation of 2.5% for 10 ignitions and this was resulted in uncertainty of ±150K and ±100K for vibrational and electron temperature, respectively. The light intensity from the OES was

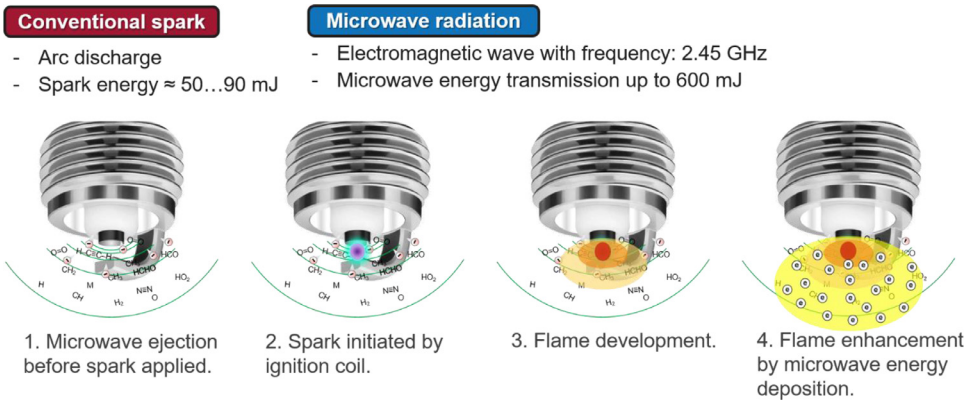

Fig. 5. Conceptual process of microwave-assisted plasma ignition.

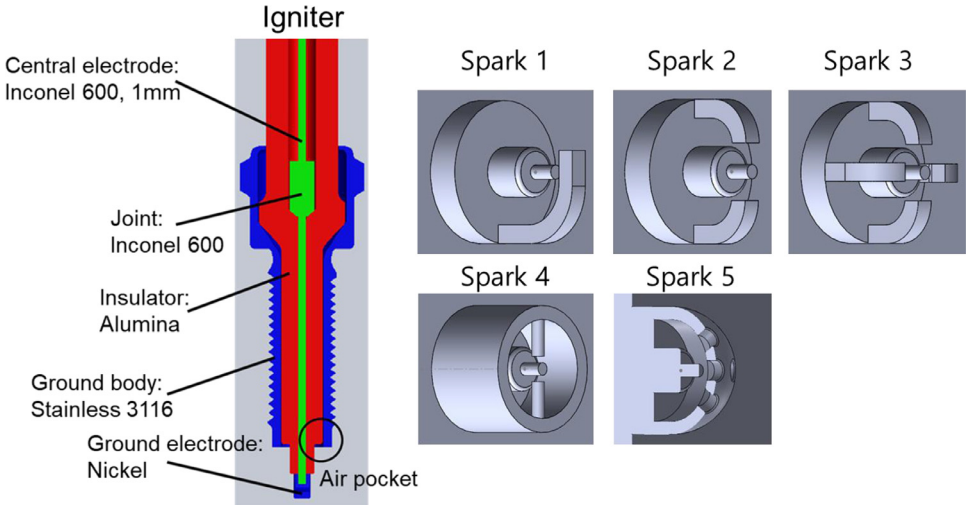

Fig. 6. Schematics of igniter tested in constant volume vessel.

further analyzed by a MATLAB based open-source SPARTAN. Using this code, the estimation of rotational (T_{rot}), vibrational (T_{vib}) and electron temperature (T_e) was carried out based on light emission theory. The spectroscopic temperature estimation code has been widely utilized in the field of plasma sciences to acquire temperature information [25, 26, 27]. The SPARTAN code can produce synthetic emission spectra with a given instrumental broadening for various molecular transitions including N_2, N_2^+, NO, OH, O_2 and also monoatomic transitions such as N, O. More details of spectroscopic models and validation can be found in [28]. The excited species were identified based on the emission band system given in [28, 29].

In the meantime, flame imaging was carried out in a constant volume vessel focusing on initial flame development. A schematic diagram of the experimental setup is shown in Fig. 7. The vessel is fabricated with carbon steel (S45C) and has 1.4L of the cubical inner section. Three quartz windows were installed at the front and two parallel side faces. A mixture of acetylene (C_2H_2) and the air was supplied with various ratios to investigate the effects of the equivalence ratio on combustion enhancement. It is known that the effect of the microwave with C_2H_2 fuel is less profound than that of CH_4 due to higher flame speed and lower activation energy [30]. However, since the autoignition and oxidation of acetylene have been intensively studied, the established data set can provide an opportunity of validation for prospective numerical simulation work [31]. The initial ambient equivalence ratio (ϕ) was controlled by the partial pressures of C_2H_2 and air with an error range of $\pm 10^{-4}$ MPa. The shadowgraph imaging was performed using two concave mirrors and a tungsten lamp in a conventional z-type setup. A high-speed camera (Phantom v7.1) equipped with a zoom lens (80–200 mm f/2.8D, Nikkor) was utilized for shadowgraph imaging that was taken with a camera setting of 20,000 frames per second (fps) in 304 by 304 pixel resolution. The exposure time and aperture of the lens were set to 2μs and 2.8, respectively. At the same time, the combustion image was also captured by an intensified charge-coupled device (ICCD) camera (PI-MAX2, Princeton Instruments) with a bandpass filter (310 nm, 67886 (V097-25), Edmund Optics) for OH radicals through the front window. The OH radical image was taken at 4ms after the start of ignition.

Images taken by high-speed shadowgraph was processed with the MATLAB program. An example image of each step is indicated in Fig. 8. First of all, the flame (Fig. 8(c)) was isolated in the image by subtracting the flame image (Fig. 8(b)) from the background image (Fig. 8(a)). Then the image was binarized (Fig. 8(d)) using a specific threshold intensity to have '0' or '1' values in the frame. An identical threshold value was applied for image analysis under every test condition. Finally, the boundary of the flame was captured by the 'boundary' function in MATLAB as shown in Fig. 8(e).

2.2.2. *Single cylinder engine*

After the fundamental investigations in the constant volume vessel, the ignition systems were implemented in a 0.5L single-cylinder GDI engine to perform combustion and emission characterization. Engine specification and test setup are shown in Table 1 and Fig. 9, respectively. The engine was operated under homogeneous-charge combustion mode that has early fuel injection timing. An electronic engine controller (ZB-9013, Zenobalti) was used to control injection parameters such as in-

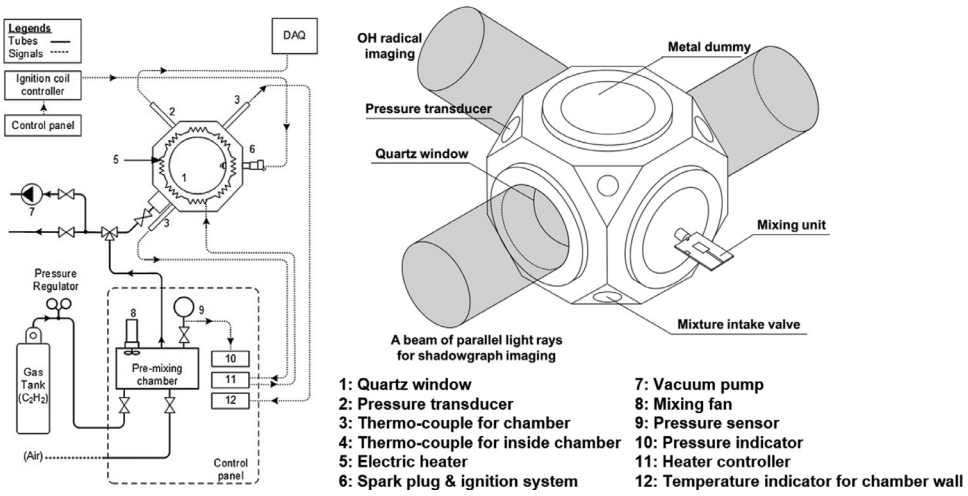

Fig. 7. Constant volume vessel system for high-speed flame imaging.

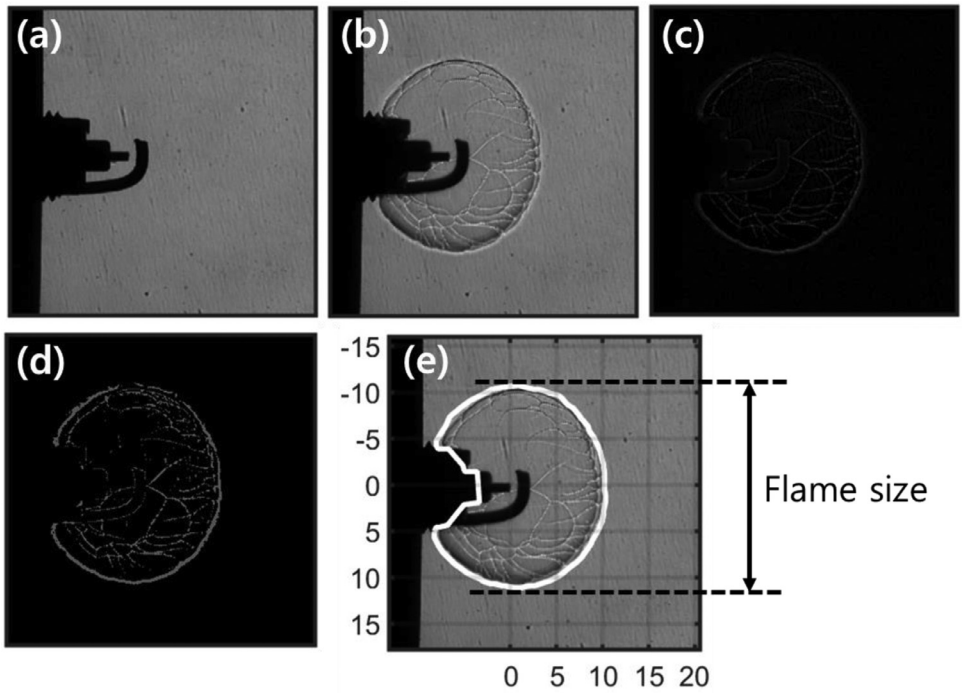

Fig. 8. Image processing for flame size measurement (a) background image, (b) flame image, (c) intensity difference (image (a)-image (b)), (d) binarization, and (e) flame size measurement

Table 1
Specifications of the test engine.

Item	Level
Number of cylinder	Single
Engine type	Spray guided direct injection, DOHC
Injector type	Piezo outward opening
Injector mount	Central mount
Bore x stroke [mm]	85 × 88
Compression ratio	12:1
Intake valve opening	11 aTDC – 22 aBDC
Exhaust valve opening	34 bBDC – 10 aTDC

jection timing, injection duration, and an injection pressure of the fuel. In-cylinder pressure was acquired using a piezoelectric pressure transducer (6052C, Kistler) coupled with a charge amplifier (5011, Kistler) with a resolution of 0.2 crank angle degree (CAD) provided by an encoder (E40S, Autonics). Heat release rate (HRR) based on in-cylinder pressure was calculated by the following equation [24].

$$\frac{dQ_n}{dt} = \frac{dQ_{ch}}{dt} - \frac{dQ_{ht}}{dt} = \frac{\gamma}{\gamma - 1} p \frac{dV}{dt} + \frac{1}{\gamma - 1} V \frac{dp}{dt} \quad (2)$$

where $\frac{dQ_n}{dt}$ is the net heat release rate, $\frac{dQ_{ch}}{dt}$ is the gross heat release rate, $\frac{dQ_{ht}}{dt}$ is the heat-transfer rate to the walls, γ is the ratio of specific heats, p is the in-cylinder pressure, V is the cylinder volume, and t is the time.

Air-fuel ratio was varied by an intake air throttling. The equivalence ratio was monitored by a lambda sensor installed in the exhaust pipe. Ensemble average of in-cylinder pressure data from 100 engine cycles was used to calculate HRR and fuel efficiency. For the emissions, CO and NO_x emissions were measured by an exhaust gas analyzer (MEXA 1500D, Horiba).

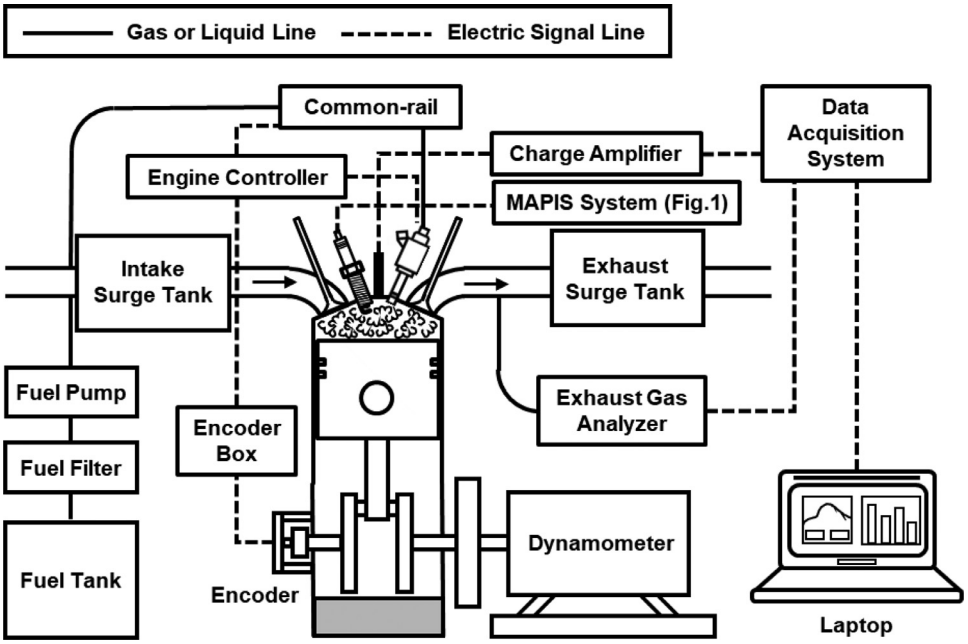

Fig. 9. Schematic diagram for single cylinder spark ignition engine system.

2.3. Test conditions

The combustion test in a constant volume vessel was conducted under a range of equivalence ratio (0.5 to 1.0) and ambient pressure (0.1 to 0.5MPa) conditions with five different spark igniters. The base spark energy and microwave application energy was set to 60mJ and 65mJ, respectively. On the other hand, the engine experiment was performed under various engine speeds from 1100 rpm to 1500 rpm. The engine load was changed from indicated mean effective pressure (IMEP) of 0.3MPa to 0.5MPa. Fuel and coolant temperatures were kept at 313K and 353K, respectively. Fuel was injected at 330CAD before top dead center (bTDC) with an injection pressure of 15MPa. The equivalence ratio was also varied from 0.63 to 1 by throttling in the intake manifold. Spark energy was set as 60mJ identical to the vessel test, however, microwave energy was changed from 65mJ to 520mJ per ignition event. Spark timing was set to have maximum brake torque (MBT) and the microwave application timing was set to 50μs earlier than the actual spark event. The summary of flame imaging and engine test conditions is tabulated in Table 2.

3. Results and discussion

3.1. Energy flow characteristics in ignition systems

Energy flows in the ignition coil and microwave system were investigated to compare system efficiency. It is noted that the voltage and current measurements were used to estimate energy flow for the ignition coil system, and the power meter was employed for the microwave system. The measurement of voltage and current in the first and second coils in the ignition coil was not feasible thus a measurement data from Bosch was used to estimate losses in each coil [32]. The result is presented in Fig. 10. In the conventional ignition system presented in Fig. 10 (a), major energy losses (~34%) occurred at primary and secondary coils. Coupling losses between primary and secondary took a minor portion (~6%) [32]. Meanwhile, in MAPIS (Fig. 10 (b)), most of the energy losses were from coupling issues in each component. This indicates that optimization of mixer and spark plug design (which was limited due to engine head design) can improve energy transfer efficiency. In terms of microwave generation, a long-term suggestion is that to modify the microwave source from magnetron to solid-state microwave generator that has ~99% efficiency. The system efficiencies of TCI and MAPIS were calculated as 53% and 13%. The estimation of energy deposition from discharge energy to flame itself is beyond the scope of this study, however, enhancement of electron temperature was investigated as in the following section.

3.2. Plasma temperature estimation from OES

The emission spectra of TCI and MAPIS is presented in Fig. 11. In Fig. 11 (a), it is shown that the vibrational transitions of nitrogen molecule (N_2), nitrogen molecule ion (N_2^+), and atomic oxygen (O1) were dominant on the emission spectrum of conventional arc discharge in ambient air condition. With microwave ejection presented Fig. 11 (b), the global intensity of emission spectrum increased approximately 8 times. Between the N2 band system, Additional reactive species were detected such as OH band at 310 nm, O2+ band at 342.1-385.9 nm and O2 Herzberg system at 345.3 nm. The emission of O1, which plays an important role in the chain-initiation process of hydrocarbon combustion, was almost doubled in intensity. The considerable increment of NO γ system emission at 231 nm also indicates the effect of microwave ejection on the excitation processes. This indicates excited electrons with microwave ejection acted as a catalyst in promoting the reaction that could not be achieved with only TCI mode.

From the measured emission spectra, the gas and electron temperatures were determined by comparing the measured spectrum with the simulated spectrum of radiative transitions. The temperature measurement technique requires a process to find a simulated spectrum with the temperatures, which shows the best match the measured spectrum. The simulated spectrum was then constructed by calculating the Boltzmann function and line broadening of selected radiative transitions with given rotational, vibrational and electronic temperature values [26, 27, 28, 33]. The dotted line in Figs. 11 (c) and (d) is experimental result and the solid line is simulation result. The solid simulation line is sum of N2+ 1- and N2 2+ as presented in fine dotted line in the figure. The temperature estimation by SPARTAN for TCI ignition in Fig. 11 (c) indicated the rotational temperature (T_{rot}) of 3,500 K, the vibrational temperature (T_{vib}) of 3,500 K and the electron temperature (T_e) of 18,000 K for TCI case. On the other hand, it showed same level of T_{rot} and T_{vib}, however, the T_e was increased to 23,000K. for MAPIS case. Distinct feature in the emission spectrum with MAPIS is that it does not follow theo-

Table 2
Experimental conditions in (a) constant volume combustion chamber, and (b) single cylinder spark ignition engine.

Item	Level
Equivalence ratio [a.u]	0.5-1.0
Initial ambient pressure [MPa]	0.1-0.5
Initial in-chamber temperature [K]	300
Spark energizing time [ms]	1
Spark energy [mJ]	60
Microwave application duration [μs]	100
Microwave application energy [mJ]	65
Microwave application timing according to spark event [μs]	-50
(a)	
Item	Level
Engine speed [r/min]	1100, 1300, 1500
Fuel injection quantity [mg/cycle]	18
Equivalence ratio [a/u.]	0.625-1
Fuel injection pressure [MPa]	15
Fuel injection timing [bTDC]	330
Spark timing	MBT
Spark energy [mJ]	60
Microwave application energy [mJ]	65-520 (0.1-0.8ms pulse duration)
Microwave application timing according to spark event [μs]	-50
Fuel temperature [K]	313
Coolant temperature [K]	353
(b)	

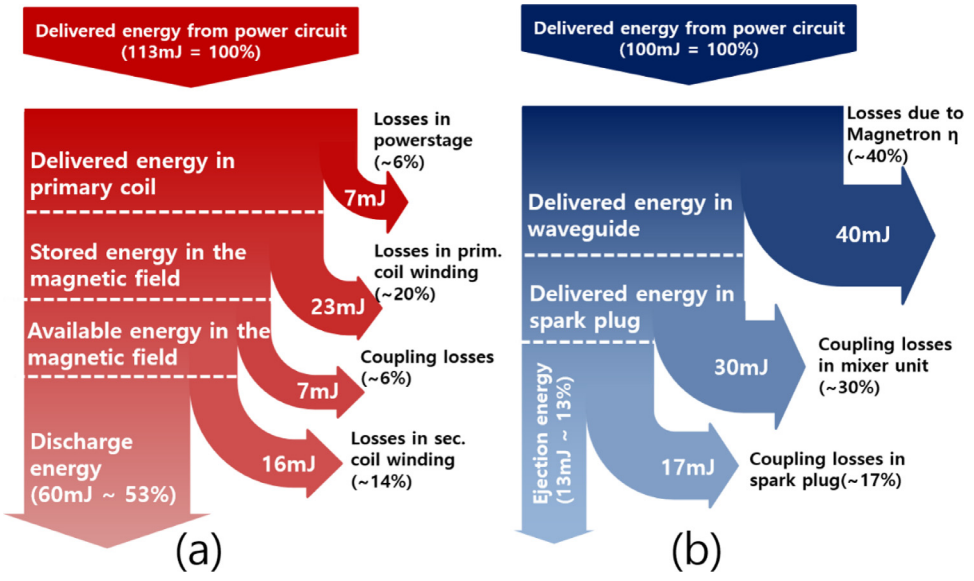

Fig. 10. Energy flow analysis on (a) conventional spark ignition, and (b) MAPIS [32].

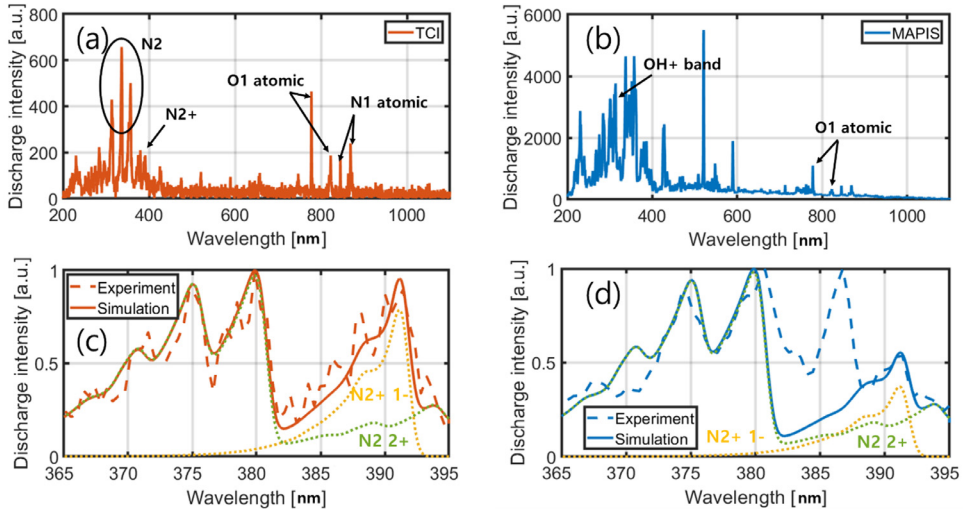

Fig. 11. Emission spectrum from (a) TCI experiment, (b) MAPIS experiment, and emission comparison by experiment and SPARTAN simulation (c) TCI, and (d) MAPIS under 0.1 MPa and air condition (results are from Spark 1).

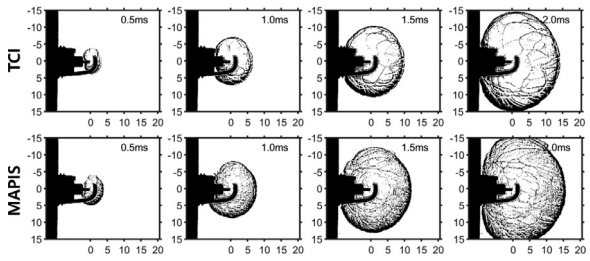

Fig. 12. Comparison of flame propagation between (a) conventional spark ignition, and (b) microwave-assisted plasma ignition under equivalence ratio of 0.8 and initial ambient pressure of 0.5 MPa.

retical Boltzmann distribution showing a high peak at 385.9 nm (O2+ emission). This implies that the plasma expansion by non-thermal mechanism was enabled by microwave ejection.

3.3. Enhancement of flame propagation with microwave ejection

Images of flame propagation using both ignition methods under a case with an ambient pressure of 0.5 MPa and an equivalence ratio of 0.8 conditions with baseline spark plug are shown in Fig. 12. As the size of the reactive plasma channel was got much greater than the conventional spark ignition case, the initial flame kernel size with microwave application got larger than conventional ignition. One interesting thing in this flame image is that the flame surface with microwave application was more wrinkled than the TCI case. One possible reason is that there would be local temperature increase or pressure gradient by electron-neutral collisions with alternating electromagnetic wave [34]. Previous researches showed that the wrinkling effect with electro-magnetic wave got intense under leaner mixture conditions [35, 36].

In terms of lean limit, the MAPIS also showed an extended lean limit in this study. As the equivalence ratio got lowered from 1.0 to 0.5, flame speed was sharply decreased, and finally, TCI showed misfire. In lean fuel-air mixture condition such as 0.5, flame propagation is not stable since it heat generation in the flame front is usually dissipated by heat low to surroundings. A relationship between heat generation in flame front and heat loss to the surrounding is presented in the following equation [37].

$$\dot{m}_F''' \Delta h_c (4\pi R_{crit}^3/3) = k(4\pi R_{crit}^2)\frac{dT}{dr}\Big|_{R_{crit}} \quad (3)$$

$$R_{crit} = \sqrt{6}\frac{\alpha}{S_L} \quad (4)$$

where, $\dot{m}_F'''$ is product generation rate per unit volume, h_c is heat of combustion, R_{crit} is critical radius, T is flame temperature, r is radius, α is thermal diffusivity, and S_L is laminar flame speed.

The correlation indicates that if the flame size is not larger than the critical flame radius, it will be dissipated as heat and finally resulted in a misfire. As presented in eq-4, the critical flame radius also can be written in a function of thermal diffusivity and laminar flame speed. The critical flame radius calculated by the correlation shows the initial flame radius should be larger than 0.12 mm, 0.54 mm for an equivalence ratio of 1.0 and 0.6, respectively. This implies that a larger size of the initial ignition kernel is required to achieve successful flame propagation under lean conditions. The TCI had misfire under the equivalence ratio of 0.5, the flame kernel could not propagate but disappeared by quenching. On the other hand, the initial flame kernel size with the microwave was much larger than the conventional ignition case and it exceeded critical flame radius so successful flame propagation was confirmed even under an equivalence ratio of 0.5. This is attributed to highly reactive radicals and electrons that were excited by an alternating electromagnetic wave. In the meanwhile, a new approach for the critical flame radius estimation can be found in the previous research of Chen et al [38]. They confirmed the correlation between critical radius/minimum ignition energy and Lewis number (*Le*) by numerical simulations showing that the critical flame radius and the minimum ignition energy increase significantly with *Le* because the positive stretch rate of the outwardly propagating flame makes the flame weaker at higher *Le*. This study suggested having lower *Le* but higher ignition energy to achieve stable flame propagation.

The OH radial distribution and intensity at the centerline are shown in Fig. 13. The color map on the right side indicated a normalized OH intensity based on the maximum OH intensity under MAPIS. The intensity at the centerline was also normalized with the maximum OH intensity with MAPIS condition. It is noted that the image was taken in the front window, so the periphery of the flame has higher intensity by the overlapping flame surfaces. The image shows an averaged flame image (from 5 ignitions) at 4ms after the actual spark event. It can be clearly seen that the OH intensity with microwave application was higher than in conventional spark case. This result is consistent with previous research that showed 6.5% higher OH-number density with microwave application [39]. This implies that chemical reactions were enhanced by electromagnetic interaction between microwave and free electrons in the flame front. The electron density of acetylene-oxygen flame at an equivalence ratio of 0.8 is known to have ~$10^{16}/m^3$, electrons could be activated by ohmic heating [40]. Many different chemical kinetics that was absent under only spark-ignition case could also be achieved by high energy electrons. In this study, the flame imaging was conducted in the quiescent initial ambient condition and fixed microwave frequency, however, the previous experimental results of Uesugi et al., using nanosecond repetitively pulsed discharge system under an ambient flow of ~10ms indicated the increase both ignition energy and discharging frequency was beneficial to achieve successful flame propagation under extreme engine-like condition [41].

3.4. Effects of electrode shape on flame development

The influence of ground electrode shape on flame enhancement under an ambient pressure of 0.5 MPa and an equivalence ratio of 0.8 conditions is presented in Fig. 14. In Fig. 14(a), the dotted and solid lines represent an outline of flame for the TCI and MAPIS system, respectively. To evaluate igniter performance, averaged flame enhancement from entire experimental conditions was calculated based on the flame propagation speed compared to the TCI case by the following equation. The flame propagation speed was acquired by dividing the difference in flame size by the time interval for the flame image.

$$Flame\ enhancement = \frac{Flame\ propagation\ speed\ with\ microwave}{Flame\ propagation\ speed\ without\ microwave}\cdot 100\ (\%) \quad (5)$$

The flame image of TCI (dotted) according to igniter geometry showed that the flame speed was enhanced with more enclosed type spark plug, for instance faster flame propagation with Spark 5 compared to Spark 1. However, it also indicated that the magnitude of flame enhancement got decreased for Spark 5 than Spark 1 based on Fig. 14(a) and Fig. 14(b). A possible reason is that as the discharge region enclosed by electrodes, flame propagation speed got higher so the actual time duration for microwave energy deposition got shorter. In other words, the effectiveness of microwave ejection was deteriorated as the flame stays shorter duration in the discharge region. The hypothesis of weaker flame enhancement with a faster flame propagation can be supported by previous work of Wolk et al., which showed an attenuation of microwave effects under fuel rich condition (fast flame propagation) than fuel lean condition (slow flame propagation) [15]. In the meanwhile, Fig. 14(c) shows the surface area of the ground electrode estimated from 3D modeling. The electrode surface area got larger as the discharge region enclosed so it can be regarded that the flame propagation of Spark 5 would be slower than Spark 1 due to greater heat losses to the ground electrode, however, in this case the structural effect played a dominant role in the flame propagation. On the other hand, the greatest improvement for

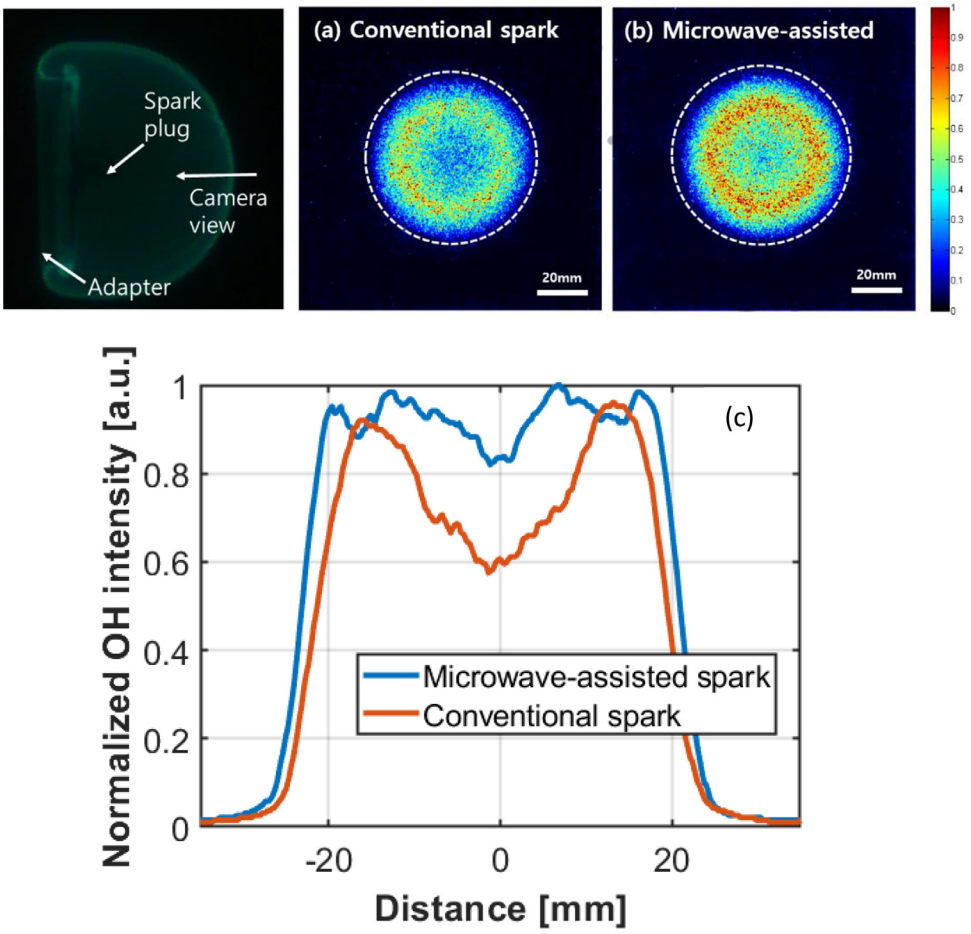

Fig. 13. Comparison of OH radical imaging from the front side under equivalence ratio of 0.8 and initial ambient pressure of 0.5 MPa using Spark 1 (a) conventional spark ignition and (b) microwave-assisted plasma ignition. The color contour was normalized by maximum OH intensity with microwave-assisted plasma ignition case. Normalized OH intensity at centerline of flame is presented in (c).

Spark 2 might be attributed to the slower flame propagation (showing smallest flame size in TCI combustion) compared to Spark 1 and larger microwave energy deposition. For further analysis of microwave influence on engine performance and emission characteristics, igniter 2 was implanted in the engine experiment.

3.5. Engine performance and emissions

The TCI and MAPIS system were applied to a single-cylinder GDI engine for performance and emission characterization. As a performance parameter, consecutive IMEP values from 100 engine cycles under an equivalence ratio of 0.75 is indicated in Fig. 15. It can be seen that the fluctuations of IMEP with microwave application was less than conventional spark case that had a misfire or partial burn showing lower IMEP than normal cycles. In the engine test, the lean limit was extended to an equivalence ratio of 0.64 whereas conventional spark ignition had misfires under an equivalence ratio of 0.8. This is because of the stronger ambient flow and more sources of heat loss in the engine system than constant volume vessel [42]. The accomplishment of stable combustion under fuel-lean condition can bring many advantages such as high fuel efficiency and low emissions that will be discussed below.

In-cylinder pressure and HRR according to microwave application energy under engine speed of 1500 rpm and engine load of 0.5 MPa is presented in Fig. 16. It is noted that the combustion phase with microwave application was earlier showing faster pressure rise and higher peak of in-cylinder pressure than TCI. The enhancement was more evident as microwave input energy increased. This is mainly due to the greater energy deposition on flame with higher microwave application cases [43]. The HRR curve, similarly to the in-cylinder pressure trace, showed a higher peak with advanced combustion phasing. The start of ignition called CA10 when cumulative heat release rate reaches 10% of total net heat release rate was approximately 3 CAD earlier with MAPIS compared to TCI. The improvement ratio of fuel efficiency compared to conventional spark ignition case is shown in Fig. 17 (a). The figure shows all of the operating points over various engine speeds (1100rpm-1500 rpm), engine load (0.3-0.5MPa), and microwave application energy (65-520mJ) conditions. As expected, based on the higher peak of in-cylinder pressure and HRR, MAPIS created more positive work so fuel efficiency was improved up to ~15% compared to conventional spark case, however, if we consider the fact of the narrow lean limit of conventional spark ignition case, the improvement was up to 6% within stable operating conditions. Based on the previous study of Wu et al., under engine condition where the *Le* is greater than quiescent condition like vessel environment, the larger gap between the electrode was beneficial for combustion stability since it can create larger initial flame kernel [44]. This result suggests a potential enhancement of MAPIS system by increasing spark plug gap.

In terms of emissions, the MAPIS took advantage of the reduction of CO emissions by ~30% compared to conventional spark conditions as shown in Fig. 17 (b). CO emissions are mainly caused by incomplete combustion or misfire during engine cycles. With microwave application, oxidation of CO emissions would be facilitated due to sufficient reactive radical pool on the flame front [45]. Based on the in-cylinder pressure and HRR, ambient gas temperature with microwave-assisted plasma ignition is expected to be higher so this also can promote faster oxidation of species from incomplete combustion. On the other hand, because of higher temperature, NO_x emissions (thermal NO_x) were increased as indicated in Fig. 17 (c). The large amount of OH or O radicals with microwave application case attributed to increase in NO_x emissions based on Zeldovich mechanism [46]. The percentage of NO_x emissions

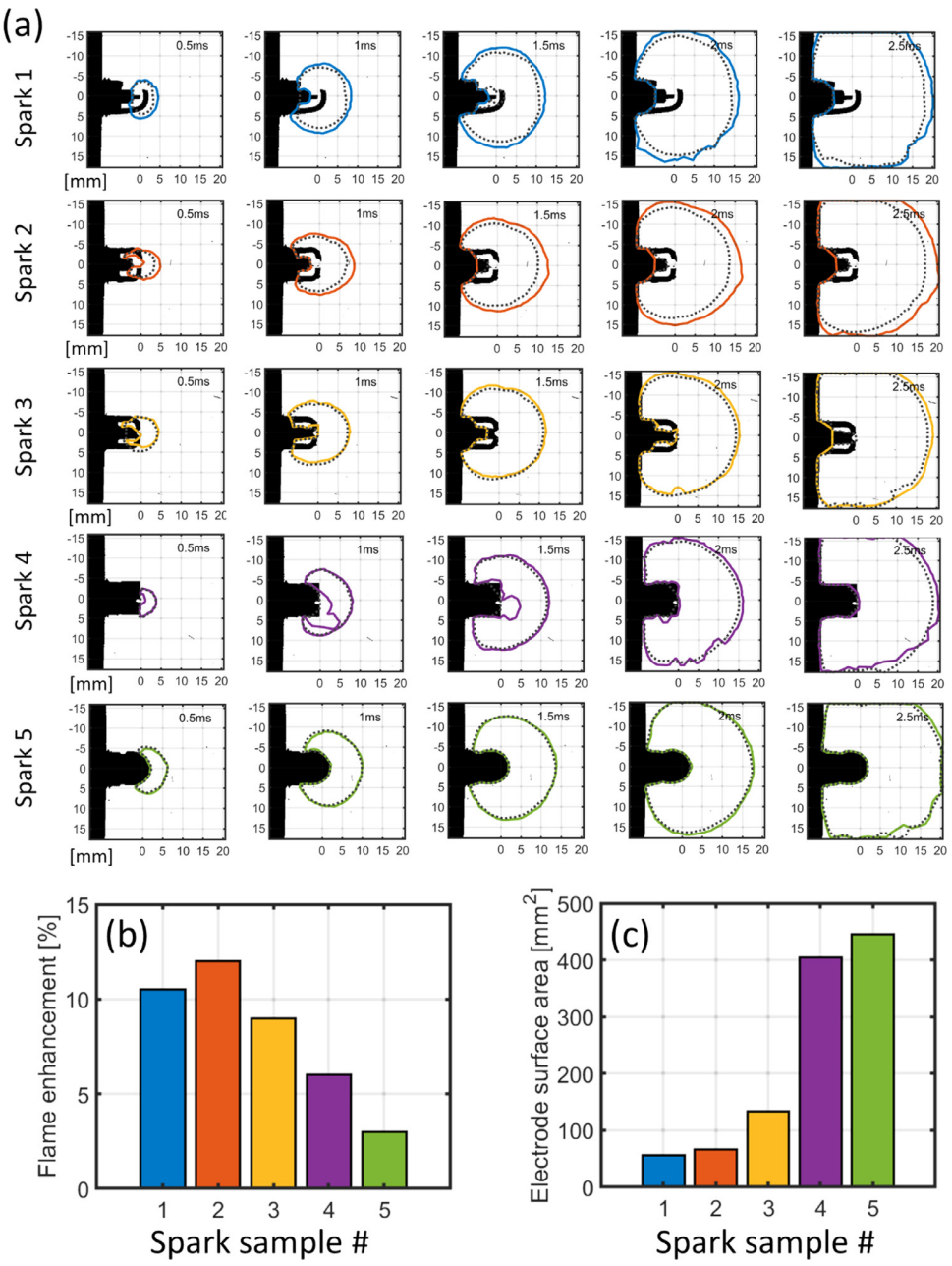

Fig. 14. Effects of electrode geometry on (a) flame propagation, (b) flame enhancement, and (c) electrode surface area.

increased under fuel-lean condition up to 2.7 times more than conventional spark case. However, even though the ratio of NO_x increase is high, the absolute level of NO_x emissions under lean condition is significantly lower than stoichiometric condition. To achieve further mitigation of NOx emissions under lean condition, a lean-NO_x trap (LNT) can be considered for microwave-assisted plasma ignition application in real vehicles [47].

Conclusions

A comprehensive assessment of flame and engine performance improvement with microwave ejection was carried out in a constant volume combustion vessel and a single-cylinder direct-injection gasoline engine. First of all, the energy balance analysis indicated that the current MAPIS has low energy transfer efficiency than TCI due to limitations in magnetron source and component design. However, the potential of flame enhancement by MAPIS was confirmed by optical emission spectroscopy (OES) and high-speed imaging. The OES result showed that the discharge with microwave does not follow theoretical Boltzmann distribution and the electron temperature was increased by 5,000K. The improvement of electron temperature and initial radical pool resulted in lean limit extension showing successful flame propagation under an equivalence ratio of 0.5. The greater initial flame kernel size and higher OH radicals were also measured with microwave application by high-speed imaging results. Based on this flame enhancement, the new ignition system took advantages of combustion stability showing much smaller variation of COV of IMEP. Stable operation under lean burn condition finally resulted in higher fuel efficiency (~6%), and reduction of CO emissions (~30%). The improvement was confirmed under various engine speed, engine load, and equivalence ratio conditions. On the other hand, NO_x emissions were higher than TCI because of elevated in-cylinder temperature. Under lean conditions, it showed 2.7 times larger NO_x emissions compared to conventional spark conditions, however, the absolute level of the emission was not considerable.

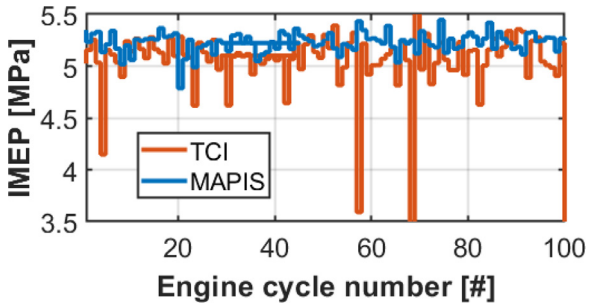

Fig. 15. Variation of IMEP during 100 cycles for conventional spark ignition and microwave-assisted plasma ignition cases at engine speed of 1500 rpm, equivalence ratio of 0.75, and IMEP of 0.5 MPa.

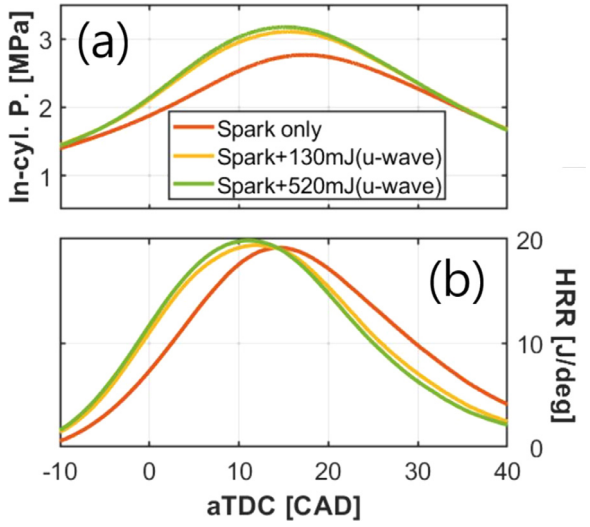

Fig. 16. Comparisons of (a) in-cylinder pressure and (b) heat release rate at engine speed of 1500 rpm, equivalence ratio of 0.75, and IMEP of 0.5 MPa.

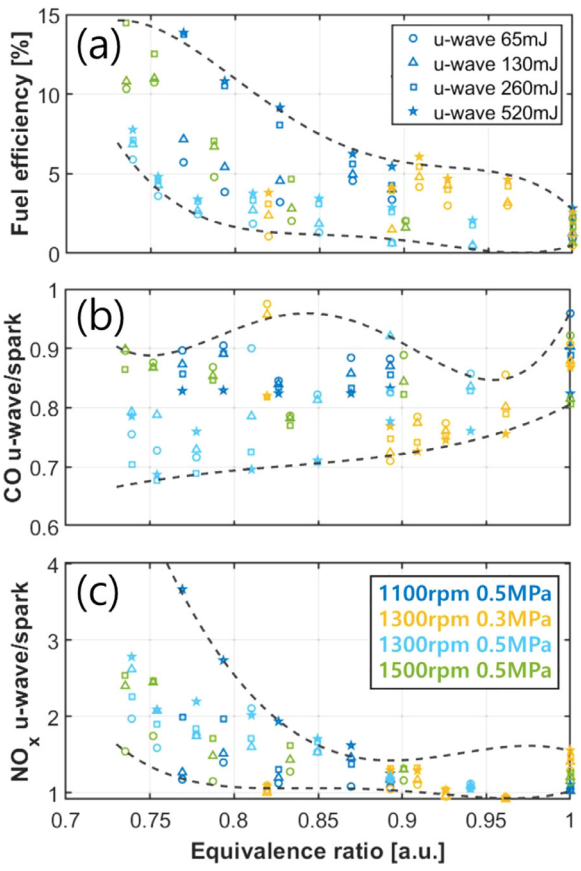

Fig. 17. Comparisons of (a) fuel efficiency improvement, (b) CO emissions, and (c) NO_x emissions according to microwave energy. Figures (b) and (c) shows ratio of microwave-assisted plasma ignition compared to conventional spark ignition case.

Declaration of Competing Interest

The authors declare that they have no known competing financial interests or personal relationships that could have appeared to influence the work reported in this paper.

Acknowledgement

The authors appreciate Hyundai Motor Company and National Research Foundation of Korea (Korea-France joint project, 2015K1A3A1A21000287) for their financial support. We also thank Dr. Jungseo Park at Zenobalti Co., Dr. Jongyoung Ahn, and Mr. Byungwook Kwon at YURA Tech Co. for providing technical support.

References

[1] Hoffmann G, Befrui B, Berndorfer A, Piock WF, Varble DL. Fuel system pressure increase for enhanced performance of GDi multi-hole injection systems. SAE Int J Engines 2014;7:519–27. doi:10.4271/2014-01-1209.
[2] Park C, Kim S, Kim H, Moriyoshi Y. Stratified lean combustion characteristics of a spray-guided combustion system in a gasoline direct injection engine. Energy 2012;41:401–7. doi:10.1016/j.energy.2012.02.060.
[3] Costa M, Sorge U, Merola S, Irimescu A, La Villetta M, Rocco V. Split injection in a homogeneous stratified gasoline direct injection engine for high combustion efficiency and low pollutants emission. Energy 2016;117:405–15. doi:10.1016/j.energy.2016.03.065.
[4] Yang J, Dong X, Wu Q, Xu M. Effects of enhanced tumble ratios on the in-cylinder performance of a gasoline direct injection optical engine. Appl Energy 2019;236:137–46. doi:10.1016/j.apenergy.2018.11.059.
[5] Wu H, Zhang F, Wang Z, Gao H. Study on initial combustion characteristics of kerosene based on inductive charging ignition system. J Phys Conf Ser 2019;1303. doi:10.1088/1742-6596/1303/1/012036.
[6] Dale JD, Checkela MD, Smyb PR. Application of high energy ignition systems to engines spark discharge and modem electrical ignition systems high energy ignition systems enhanced ignition systems 5.1. Breakdown and laser ignition systems, corona spark plug 5.2. Plasma jet and rail plug. Prog Energy Combusr Sci 1997;23:379–98.
[7] Kobayashi T, Yamaki Y, Nakaya S, Tsue M. Influences of multi spark discharge on lean ignition for premixed propane/air mixtures under turbulent environment. SAE Tech Pap 2019:7191. doi:10.4271/2019-01-2161.
[8] Mariani A, Foucher F. Radio frequency spark plug: an ignition system for modern internal combustion engines. Appl Energy 2014;122:151–61. doi:10.1016/j.apenergy.2014.02.009.
[9] Sjöberg M, Zeng W, Singleton D, Sanders JM, Gundersen MA. Combined effects of multi-pulse transient plasma ignition and intake heating on lean limits of well-mixed E85 DISI engine operation. SAE Int J Engines 2014;7:1781–801. doi:10.4271/2014-01-2615.
[10] Shiraishi T, Urushihara T. Fundamental analysis of combustion initiation characteristics of low temperature plasma ignition for internal combustion gasoline engine. SAE Tech Pap 2011.
[11] Anokhin EM, Kuzmenko DN, Kindysheva SV, Soloviev VR, Aleksandrov NL. Ignition of hydrocarbon : air mixtures by a nanosecond surface dielectric barrier discharge. Plasma Sources Sci Technol 2015;24. doi:10.1088/0963-0252/24/4/045014.
[12] Defilippo A, Saxena S, Rapp V, Dibble R, Chen JY, Nishiyama A, et al. Extending the lean stability limits of gasoline using a microwave-assisted spark plug. SAE Tech Pap 2011:7191.
[13] Ikeda Y, Nishiyama A, Katano H, Kaneko M, Jeong H. Research and development of microwave plasma combustion engine (Part II: Engine performance of plasma combustion engine). SAE Tech Pap 2009. doi:10.4271/2009-01-1049.
[14] Padala S, Nishiyama A, Ikeda Y. Flame size measurements of premixed propane-air mixtures ignited by microwave-enhanced plasma. Proc Combust Inst 2017;36:4113–19. doi:10.1016/j.proci.2016.06.168.
[15] Wolk B, DeFilippo A, Chen JY, Dibble R, Nishiyama A, Ikeda Y. Enhancement of flame development by microwave-assisted spark ignition in constant volume combustion chamber. Combust Flame 2013;160:1225–34. doi:10.1016/j.combustflame.2013.02.004.
[16] Le MK, Nishiyama A, Serizawa T, Ikeda Y. Applications of a multi-point microwave discharge igniter in a multi-cylinder gasoline engine. Proc Combust Inst 2019;37:5621–8. doi:10.1016/j.proci.2018.06.033.

[17] Starikovskiy A, Aleksandrov N. Plasma-assisted ignition and combustion. Prog Energy Combust Sci 2013;39:61–110. doi:10.1016/j.pecs.2012.05.003.
[18] Ju Y, Sun W. Plasma assisted combustion: dynamics and chemistry. Prog Energy Combust Sci 2015;48:21–83. doi:10.1016/j.pecs.2014.12.002.
[19] Hwang J, Kim W, Bae C, Choe W, Cha J, Woo S. Application of a novel microwave-assisted plasma ignition system in a direct injection gasoline engine. Appl Energy 2017;205:562–76. doi:10.1016/j.apenergy.2017.07.129.
[20] Ikeda Y, Nishiyama A, Kaneko M. Microwave enhanced ignition process for fuel mixture at elevated pressure of 1MPa. 47th AIAA Aerosp Sci Meet Incl New Horiz. Forum Aerosp Expo 2009:1–12. doi:10.2514/6.2009-223.
[21] Nishiyama A, Ikeda Y. Improvement of lean limit and fuel consumption using microwave plasma ignition technology. SAE Tech Pap 2012. doi:10.4271/2012-01-1139.
[22] Thostenson ET, Chou TW. Microwave processing: fundamentals and applications. Compos Part A Appl Sci Manuf 1999;30:1055–71. doi:10.1016/S1359-835X(99)00020-2.
[23] Brittain JE. The magnetron and the beginnings of the microwave age. Phys Today 1985;38:60–7. doi:10.1063/1.880982.
[24] Heywood JB. Internal combustion engine fundamentals. Choice Rev Online 1988;26 26-0943-26–0943. doi:10.5860/choice.26-0943.
[25] Bruggeman PJ, Sadeghi N, Schram DC, Linss V. Gas temperature determination from rotational lines in non-equilibrium plasmas: a review. Plasma Sources Sci Technol 2014;23. doi:10.1088/0963-0252/23/2/023001.
[26] Moon SY, Choe W. A comparative study of rotational temperatures using diatomic OH, O2 and N2+ molecular spectra emitted from atmospheric plasmas. Spectrochim Acta - Part B Spectrosc 2003;58:249–57. doi:10.1016/S0584-8547(02)00259-8.
[27] Laux CO, Spence TG, Kruger CH, Zare RN. Optical diagnostics of atmospheric pressure air plasmas. Plasma Sources Sci Technol 2003;12:125–38. doi:10.1088/0963-0252/12/2/301.
[28] Lino da Silva M. An adaptive line-by-line-statistical model for fast and accurate spectral simulations in low-pressure plasmas. J Quant Spectrosc Radiat Transf 2007;108:106–25. doi:10.1016/j.jqsrt.2007.03.005.
[29] Pearse RWB, Gaydon AG. The identification of molecular spectra. Identif Mol Spectra 1976. doi:10.1007/978-94-009-5758-9.
[30] Kosarev IN, Kindysheva SV, Aleksandrov NL, Starikovskiy AY. Ignition of ethanol-containing mixtures excited by nanosecond discharge above self-ignition threshold. Combust Flame 2015;162:50–9. doi:10.1016/j.combustflame.2014.07.014.
[31] Kosarev IN, Pakhomov AI, Kindysheva SV, Anokhin EM, Aleksandrov NL. Nanosecond discharge ignition in acetylene-containing mixtures. Plasma Sources Sci Technol 2013;22. doi:10.1088/0963-0252/22/4/045018.
[32] Schneider A, Hettinger A, Kufferath A, Rottengruber H. 2 Requirements of Inductive Ignition Systems under Engine and Steady-State Conditions; 2014. 2014.
[33] Whiting EE, Chul P, Liu Y, Arnold O, Paterson A., NEQAIR96, nonequilibrium and equilibrium radiative transport and spectra program: user's manual 1996:1–170.
[34] Dysthe KB, Mjøflhus E, Pécseli HL, Rypdal K. A thermal oscillating two-stream instability. Phys Fluids 1983;26:146–57. doi:10.1063/1.863993.
[35] Marcum SD, Ganguly BN. Electric-field-induced flame speed modification. Combust Flame 2005;143:27–36. doi:10.1016/j.combustflame.2005.04.008.
[36] Wisman DL, Marcum SD, Ganguly BN. Electrical control of the thermodiffusive instability in premixed propane-air flames. Combust Flame 2007;151:639–48. doi:10.1016/j.combustflame.2007.06.021.
[37] Turns SR. An Introduction to Combustion. System 2000;499:1–676.
[38] Chen Z, Burke MP, Ju Y. On the critical flame radius and minimum ignition energy for spherical flame initiation. Proc Combust Inst 2011;33:1219–26. doi:10.1016/j.proci.2010.05.005.
[39] Stockman ES, Zaidi SH, Miles RB, Carter CD, Ryan MD. Measurements of combustion properties in a microwave enhanced flame. Combust Flame 2009;156:1453–61. doi:10.1016/j.combustflame.2009.02.006.
[40] Shuler KE, Weber J. A microwave investigation of the ionization of hydrogen-oxygen and acetylene-oxygen flames. J Chem Phys 1954;22:491–502. doi:10.1063/1.1740095.
[41] Uesugi K, Morii Y, Mukoyama T, Tezuka T, Hasegawa S, Nakamura H, et al. Ignition experiments by nanosecond repetitively pulsed discharges in intense turbulence for super lean burn at engine condition. SAE Tech Pap 2019:1–6. doi:10.4271/2019-01-2160.
[42] Peterson B, Reuss DL, Sick V. High-speed imaging analysis of misfires in a spray-guided direct injection engine. Proc Combust Inst 2011;33:3089–96. doi:10.1016/j.proci.2010.07.079.
[43] Michael JB, Chng TL, Miles RB. Sustained propagation of ultra-lean methane/air flames with pulsed microwave energy deposition. Combust Flame 2013;160:796–807. doi:10.1016/j.combustflame.2012.12.006.
[44] Wu F, Saha A, Chaudhuri S, Law CK. Facilitated ignition in turbulence through differential diffusion. Phys Rev Lett 2014;113:1–5. doi:10.1103/PhysRevLett.113.024503.
[45] Biswas S, Ekoto I. Detailed investigation into the effect of ozone addition on spark assisted compression ignition engine performance and emissions characteristics. SAE Tech Pap 2019 2019-April. doi:10.4271/2019-01-0966.
[46] Bowman CT. Kinetics of pollutant formation and destruction in combustion. Prog Energy Combust Sci 1975;1:33–45. doi:10.1016/0360-1285(75)90005-2.
[47] Theses M, Trace Williams AM. Tennessee research and creative exchange lean NOx trap catalysis for lean burn natural gas engines; 2004.